EasyChair Preprint

№ 10613

Cup-Disk Ratio Segmentation Joint with Key Retinal Vascular Information Under Diagnostic and Screening Scenarios

Kuo Yang, Wenhao Jiang, Yiqiao Shi, Rui Qin, Wanli Bai, Duo Li, Yue Wu and Menghan Hu

July 24, 2023

CGI2023 manuscript No.
(will be inserted by the editor)

Cup-disk ratio segmentation joint with key retinal vascular information under diagnostic and screening scenarios

Kuo Yang[†] · Wenhao Jiang[†] · Yiqiao Shi · Rui Qin · Wanli Bai · Duo Li · Yue Wu[*] · Menghan Hu[*]

Abstract Glaucoma is one of the leading causes of irreversible blindness worldwide. Numerous studies have shown that a larger vertical Cup-to-Disc Ratio (CDR) is closely associated with the glaucoma diagnosis. CDR is highly useful in the clinical practice and evaluation of glaucoma. However, the determination of CDR varies among clinicians and is highly dependent on the doctor's subjectivity. Existing methods only segment the cup and disc features without considering the nearby vascular information. Based on guidance and criteria from experienced clinicians in diagnosing glaucoma, we incorporate segmented essential vascular information to constrain CDR segmentation. We add key vessel information to the network as the prior knowledge to better guide the model to distinguish the boundary of the optic cup. The effectiveness of incorporating essential vascular information has been demonstrated through experiments conducted on the public dataset REFUGE as well as the home-made dataset. The home-made dataset consists of high-quality CDR images and remade CDR images, corresponding to the diagnosis scenario and the screening scenario in which the patient needs to upload the fundus image by taking photos. The model is deployed on the Wechat mini-program for practical glaucoma diagnostic and screening applications.

Keywords Cup-disk ratio segmentation · Retinal vascular · Glaucoma diagnostic and screening

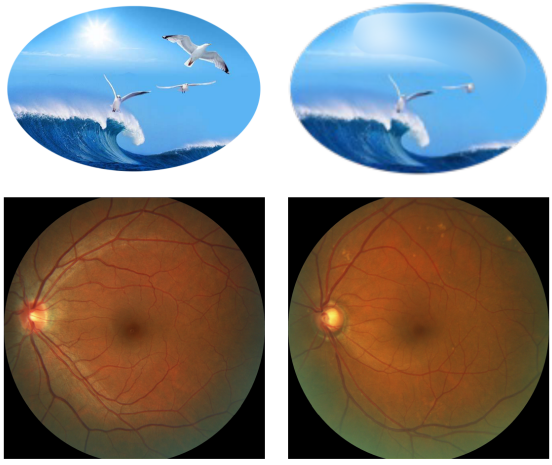

(a) Non-Glaucoma (b) Glaucoma

Fig. 1 Top image illustrates the difference in visual fields between non-glaucoma and glaucoma patients [1]. Glaucoma patients often experience blurry vision and visual field loss. The images below are from the REFUGE dataset, with the left showing a non-glaucomatous retinal image and the right showing a glaucomatous retinal image.

1 Introduction

Glaucoma is currently the leading cause of irreversible blindness worldwide [2], and it is one of the major causes of irreversible vision loss in the world. It has a high prevalence and blindness rate. According to estimates by the World Health Organization, the number of glaucoma patients worldwide exceeded 88 million in 2020

Kuo Yang, Wenhao Jiang, Yiqiao Shi, Rui Qin, Wanli Bai, Menghan Hu
Shanghai Key Laboratory of Multidimensional Information Processing, East China Normal University, China.

Yue Wu
Department of Ophthalmology, Ninth People's Hospital Affiliated to Shanghai Jiao Tong University School of Medicine, China.

Duo Li
DiDi Chuxing, China.
Corresponding authors: Yue Wu (wuyue@shsmu.edu.cn), Menghan Hu (mhhu@ce.ecnu.edu.cn)
[†]These authors contributed equally to this work.

[3]. The progression of glaucoma is initially asymptomatic and gradually leads to vision loss, which can only be observed in the late stage. Once diagnosed, it results in permanent visual impairment. Early detection and timely treatment of glaucoma can further control disease progression, making it an important means of preventing glaucoma [4][5]. It is usually caused by elevated intraocular pressure (IOP), which leads to mechanical strain and torsion of the optic nerve, as well as loss of retinal nerve fibers. Glaucoma alters the morphology of the optic nerve head (ONH), typically manifesting as a larger CDR, pale optic disc, disc hemorrhage, etc. Digital fundus imaging is an important medical tool that assists doctors in diagnosing and analyzing glaucoma [6][7]. Fundus images include various features of the fundus area, such as the optic disc, cup, arterioles, and venules. As shown in Figure 1, the visual field of a normal individual and that observed by glaucoma patients differ [8].

In digital fundus images, the optic disc (OD) appears as a pale yellow region, and within the OD, there is a relatively bright elliptical or circular area called the optic cup (OC). The CDR, which represents the ratio of the size of the central depression to the size of the OD, is an important auxiliary parameter for glaucoma diagnosis. Clinicians identify the specific boundaries of the OD and OC and calculate the corresponding ratio to assist in determining whether it is glaucoma. Although both the OC and disc exist in normal individuals, the area or diameter ratio of the OD and OC in glaucoma patients' fundus images is higher than that of normal individuals. Due to elevated IOP, the size of the OC is larger than that of normal individuals. Therefore, when the vertical CDR ratio exceeds 0.65 [9], the patient is classified as having glaucoma according to clinical standards.

Since doctors need to manually segment the OD and OC regions in fundus images and estimate the approximate CDR value for classification, this glaucoma diagnosis method requires a considerable amount of manual effort, is time-consuming, and inefficient. Moreover, it depends to some extent on the expertise of ophthalmologists, and the information extracted manually from fundus images is limited. Therefore, computer-assisted medical diagnosis is of paramount importance.

In recent years, there have been numerous efforts to utilize computer-aided medical diagnosis, broadly categorized into traditional methods and deep learning methods. Traditional methods include approaches based on color, contrast thresholds, and morphological operations on the OD. These traditional methods are sensitive to image quality and pathological variations, resulting in low accuracy. Studies have employed edge

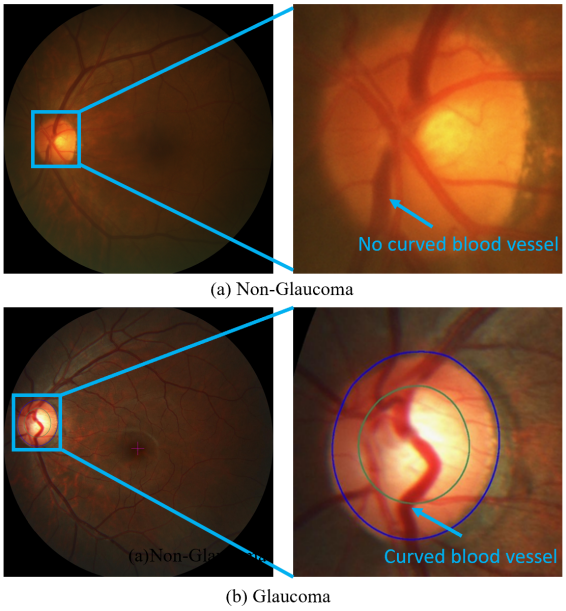

Fig. 2 Fundus images of non-glaucoma and glaucoma. (a) depicts a glaucomatous retinal image where VC, primarily concentrated at the OD and OC boundaries, is caused by glaucoma. In non-glaucoma fundus images as (b), the blood vessels at the boundary are not curved.

detection methods to segment the OD and OC, assuming clear boundaries between them. Nevertheless, in certain cases, the boundaries may be indistinct, leading to inaccurate segmentation. Machine learning algorithms have also been applied to the OD and OC segmentation, relying on manual feature extraction and lacking the ability to automatically learn complex features.

Significant progress has been made in OD and OC segmentation using deep learning methods [10][11][12]. These approaches employ convolutional neural networks (CNNs) [13][14] to learn complex features from input images. Studies use CNNs with encoder-decoder structures, such as U-Net [15] and Mask R-CNN [16], for OD and OC segmentation. These methods have achieved high accuracy, but they still face challenges in accurately segmenting the boundaries between the OD and OC. This is because blood vessels near the fundus can influence the OD and OC segmentation, causing the models to struggle with precise boundary delineation.

Existing methods for CDR segmentation do not consider the information from blood vessels in the segmentation of the OD and OC. Based on the clinical experience of expert ophthalmologists, in the segmentation of CDR for glaucoma, doctors pay attention to the curvature of blood vessels within the OC to determine the boundary of the OC. As shown in the Figure 2, there is a curvature in the blood vessels of glaucoma, and

doctors use the location of vessel curvature to assist in determining the boundary of the OC.

Motivated by this observation, we incorporate the information of retinal blood vessels into the network for learning. By learning the prior information about blood vessels through the network, we aim to assist in the segmentation of the OD and OC. We introduce the concept of Vascular Curvature (VC), as VC can affect the boundaries of the OD and OC. If the model can utilize this vessel information to assist in the OD and OC segmentation, similar to how clinicians do, the performance of CDR segmentation can be improved. Therefore, we define how blood vessels in retinal images impact the OD and OC segmentation, as well as the VC degree. We incorporate the VC information into the model to enable it to learn the vessel information that affects the boundaries of the disc, thereby assisting in the OD and OC segmentation.

2 Related Work

Lalonde et al. initially proposed a template matching-based approach to obtain the boundary of the OD [17]. Since the shape of the OD and OC [18] is generally elliptical or circular, the method segments the OD and OC by extracting the edges of the retinal image and matching them with a template [19][20][21]. Due to the heavy reliance on template matching, the method suffers from poor performance when the shape of the boundary is affected by the surrounding blood vessels. Mendels et al. employed a contour model to detect the boundary of the OD based on image gradients [22][23][24]. To suppress the influence of blood vessels on the boundary, an active contour model based on Gradient Vector Flow (GVF) was used for disc boundary detection, followed by minimizing the high gradients caused by vessel locations to reduce the impact [25][26]. Lowell et al. employed circular transform techniques to obtain the boundary of the OD [27][28]. The segmentation of the OC, which is located within the disc and has low contrast, poses a greater challenge. Li et al. proposed a variational level set-based algorithm for OD segmentation, utilizing ellipse fitting operations for smoothing to obtain the segmentation result of the disc [29]. Li et al. represented features for OC segmentation based on visual characteristics such as color histograms [30]. Relying on manually extracted features, the method heavily depends on image quality and the position of pathological regions, resulting in poor robustness. Wong et al. first discovered the usefulness of vessel tortuosity for OC segmentation [20], but did not consider the influence of natural vessel curvature around the OC. There are also some methods [31][32][33] combining vascular information that do not solve the OD and OC segmentation problem. Sevastopolsky et al. proposed a modified U-Net for OD and OC segmentation [34], but did not perform joint OD and OC segmentation, instead separating them in a sequential manner. Zilly et al. proposed an integrated learning method based on CNN for OC and OD extraction [35].

3 Methods

3.1 Background

Our goal is to address the CDR measurement in real glaucoma diagnosis and screening scenarios. Directly applying models trained on public datasets to real-world applications results in poorer performance due to the inherent blurriness of images in screening scenarios compared to the original fundus images. To better align with real-world application scenarios, we not only require the original fundus images as data for glaucoma diagnosis, but also incorporate user-uploaded fundus images taken manually during the screening process into the training set. We collect 400 images captured by users from different angles using mobile phones during the glaucoma screening phase, which are included as part of the training set. Additionally, we performed joint training using the REFUGE dataset, which represents the diagnostic scenario.

3.2 Data preprocessing

For semantic segmentation using deep learning methods, data plays a crucial role. Previous studies have utilized retinal datasets such as REFUGE [21], ORIGA [36], Drishti [37], and others. These datasets consist of images captured using professional equipment and annotated by experts, ensuring high data quality and relieving the pressure on neural networks to learn from them. To address the issues of model overfitting and poor generalization caused by limited data, researchers employ various data augmentation techniques to enhance model performance. In real-world scenarios, acquiring high-quality datasets is challenging, making data preprocessing even more important.

The ultimate goal is to apply this model to real clinical diagnostics and screenings. Existing methods perform well on publicly available datasets such as REFUGE, but they often struggle with generalization in real-world diagnostic and screening scenarios. Various factors and conditions can impact the performance of existing algorithms in practical applications. To enhance the model's

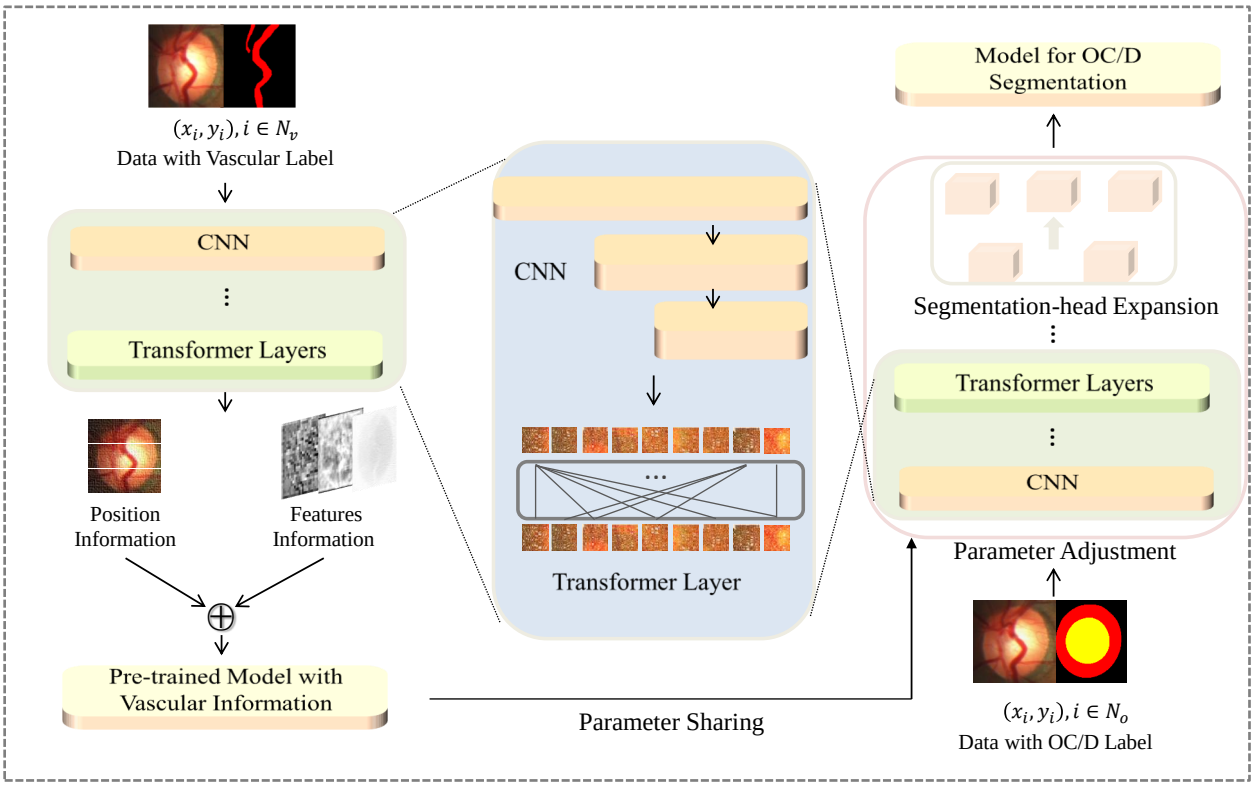

Fig. 3 Overall framework for CDR segmentation. In this diagram, we describe the entire process of the model. We first pre-train the model using vascular data, then transfer learning on OC and OD data, and expand the classification head for new tasks.

generalization, we include images collected during actual diagnostic processes as part of the dataset and perform joint training with the REFUGE dataset. This approach better aligns with the requirements and scenarios encountered in real-world applications.

In this work, we employ object detection algorithms to locate the OD region in retinal images and crop fixed-size regions to reduce interference from complex backgrounds and noise. Since we emphasize the learning of vascular information and useful VC information is primarily present within the OD region, cropping the region of interest may aid in learning vessel information and the OD and OC segmentation. Additionally, some retinal datasets provide only annotations for the OD and OC without corresponding vessel information. To strengthen the influence of vessels, two approaches can be adopted: explicit intervention and implicit intervention.

In this task, explicit intervention refers to directly utilizing the position information of VC as the criterion for OC segmentation. For example, we employ feature point detection or curvature calculation to obtain VC information and use it as the boundary for the OC. Such an approach overlooks the impact of other important information in retinal images on OC segmentation. In complex vessel scenarios, this judgment method poses a significant challenge to the model robustness. The impressive performance demonstrated by neural networks leads us to believe that they are capable of learning hierarchical feature information from retinal images and considering it comprehensively. Therefore, we adopt an implicit intervention approach, providing label information for vessels that influence the boundary of the OC in retinal images, thereby enhancing the network's ability to discriminate vessels and making VC information one of the key factors improving the final segmentation results.

Table 1 Experimental results. We conduct joint training on the REFUGE dataset and the GSD dataset separately using the U-Net [15], TransU-Net [38], Segtran [39] architecture. This process yields models that are subsequently utilized to make predictions on both the REFUGE dataset and the GSD dataset. *VC* represents only critical vascular information.

	REFUGE			GSD		
	Dice (OD)	Dice (OC)	Average dice	Dice (OD)	Dice (OC)	Average dice
U-Net [15]	0.873	0.805	0.839	0.490	0.715	0.603
U-Net with VC	**0.927**	**0.819**	**0.873**	**0.872**	**0.813**	**0.843**
TransU-Net [38]	0.958	0.900	0.929	0.899	0.801	0.850
TransU-Net with VC	0.956	**0.901**	0.929	**0.913**	**0.819**	**0.859**
Segtran [39]	0.870	0.835	0.853	0.917	0.849	0.883
Segtran with VC	**0.895**	**0.841**	**0.868**	**0.942**	0.845	**0.894**

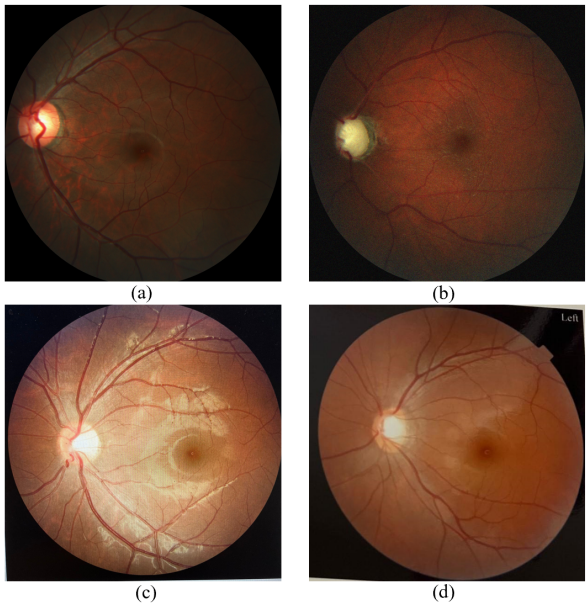

Fig. 4 Typical examples in GSD dataset. (a) represents the original retinal image, (b) displays the retinal image with added noise, (c) shows screen-captured images, and (d) exhibits retinal images uploaded by portable devices such as mobile phones or tablets.

3.3 Blood vessel feature extraction and information fusion

After implicitly introducing VC information, we divide the entire training process into two parts. In the first step, the network learns vessel information from retinal images. Convolutional neural network based methods have achieved remarkable results for vessel segmentation. The label information provides for retinal images contains only a portion of vessels that may affect the OC boundary, which may lead to fragmented vessel states and higher requirements for positional information. While CNN demonstrates powerful feature extraction capabilities and can handle most vessel segmentation tasks, it falls short compared to Transformers in capturing contextual information and extracting global information. To enable the network to better learn crucial vessel information, we adopt a network that combines CNN and Transformers, as shown in Figure 3. The original image undergoes CNN to obtain feature distribution data, which is then combined with positional information and fed into the Transformer. This combination leverages the strengths of both CNN and Transformers to enhance the acquisition of specific vessel information. Notably, the incorporation of vascular information fundamentally serves as prior knowledge for model learning. The selection of different network architectures leads to variations in the final results, which can be categorized as horizontal comparisons. The vertical enhancement brings by vascular information proves effective for CNNs as well, providing a novel perspective primarily aims at improving the OD and OC segmentation performance.

After fully learning vessel information from retinal images, a key challenge is how to incorporate it into the OD and OC segmentation task. As mentioned earlier, the implicit intervention approach embeds vessel information in the model, allowing us to utilize this knowledge as prior information for guiding the model in learning OD and OC segmentation. Previous work has demonstrated the effectiveness of transfer learning using pre-trained models. The challenges we face are similar yet distinct. Transfer learning primarily involves pre-training on large-scale datasets to obtain powerful

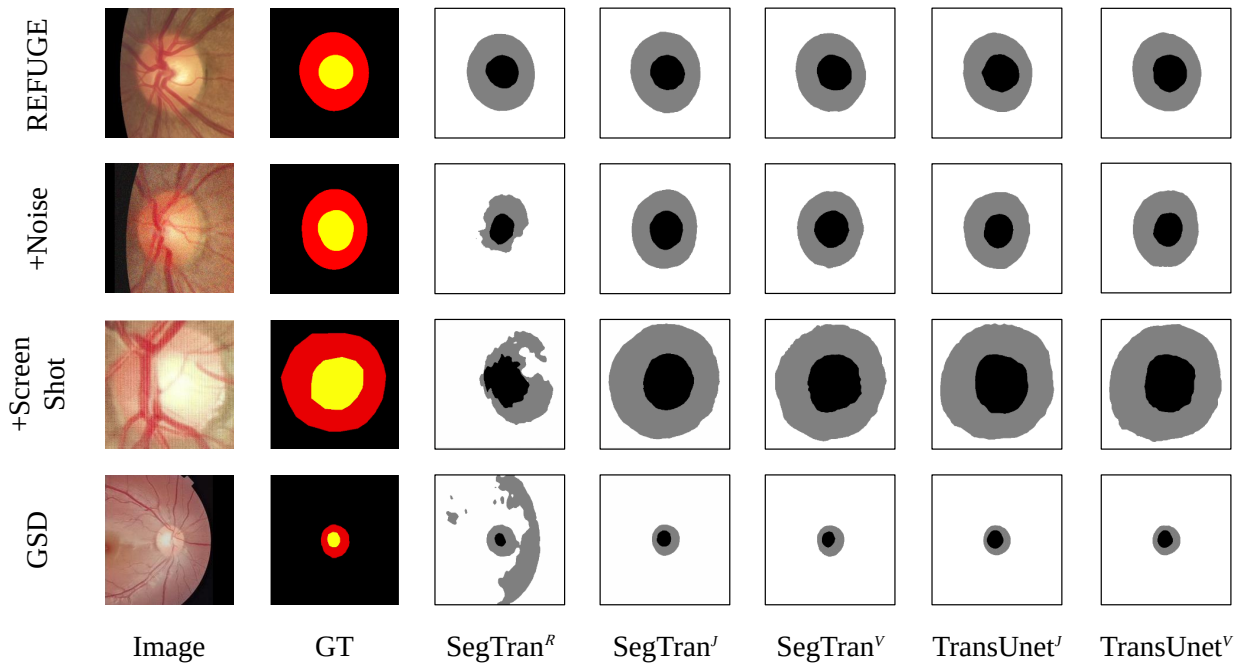

Fig. 5 Comparison of model performance. Input consists of fundus photos from four different scenes; GT refers to the pre-annotated ground truth; The rest is the result of Segtran [36] prediction visualization under different dataset and different conditions. R represents the model trained on REFUGE dataset, J represents the model jointly trained on REFUGE and GSD dataset, and V represents the model obtained by adding key blood vessel information and jointly trained.

feature extraction models and achieve excellent performance on downstream tasks. In contrast, the data we train on the pre-training and fine-tuning stages lack such features, and thus, factors improving the final performance mainly stem from the prior knowledge provided by vessels. We use the vessel information learning model as a pre-trained model and fine-tune it on the new OD and OC segmentation task. Given the significant differences between the two tasks, to preserve the guiding function of vessel information, we need to consider retaining information from the old task while adjusting to the new task. We transfer the feature extraction component from the existing vascular model to a new model, while incorporating a novel classification head for the new model. Moreover, we adopt a lower learning rate to ensure a smooth transition from old knowledge to new knowledge.

4 Experiment

4.1 Dataset

GSD: GSD dataset is collected for Glaucoma Screening and Diagnosis. We collect a dataset consisting of images specifically acquired for glaucoma screening and diagnosis. The real screening scenario comprises 400 images captured during actual clinical procedures. Images taken toward a screen may exhibit variations in clarity and angles due to differences in shooting angles and imaging devices. The dataset collects under various conditions aligns with real-world scenarios encountered in clinical practice. In addition to the data presented above, we have collected some additional processed data. Among them, 400 images are captured from the screen with reference to the REFUGE dataset, and 200 images are artificially augmented with noise on the REFUGE dataset, including Gaussian noise, contrast adjustment, brightness conversion and other operations. Some typical examples of the GSD dataset are shown in Figure 4.

REFUGE: It consists of a dataset of 400 images for OD and OC segmentation, including 40 images of glaucomatous fundus and 360 images of non-glaucomatous fundus with different sizes and resolutions.

4.2 Experimental setting

To assess the impact of data quantity in different scenarios on the model, we add 200 noisy images created by introducing noise to the original images in the dataset.

Table 2 Ablation study results. To verify the validity of blood vessel information on the model, we add all blood vessel information and only key blood vessel information into the model for training, and make predictions on REFUGE and GSD datasets. V represents all vascular information, and VC represents only critical vascular information. The result is the average Dice of all data.

Methods	Dice (OD)	Dice (OC)	Average dice
U-Net [15]	0.682	0.760	0.721
U-Net with all V	0.490	0.715	0.603
U-Net with VC	**0.900**	**0.816**	**0.858**
Segtran [39]	0.848	0.834	0.841
Segtran with all V	0.820	0.811	0.816
Segtran with VC	**0.936**	**0.846**	**0.891**

Using an initial model as the pre-training model, we select 75% of the retinal fundus photographs from each respective scenario as the training set and performed joint training on retinal fundus photographs from different scenarios, resulting in the current model. To enhance user experience, we incorporate functionalities for retinal photograph localization and automatic classification of left and right eyes. The experimental results are shown in Figure 5.

To evaluate the performance of the model, we use the remaining 25% of the dataset as the test set, including 100 original images from REFUGE dataset, 50 images with added noise, 100 images captured from screens, and 100 actual diagnostic images. We conduct separate tests on the initial model trained on REFUGE dataset and the existing model trained on retinal fundus photographs from multiple scenarios. The test results are presented in Table 1, and a subset of actual segmentation results is shown in Figure 5. The dice coefficient serves as an evaluation metric for image segmentation.

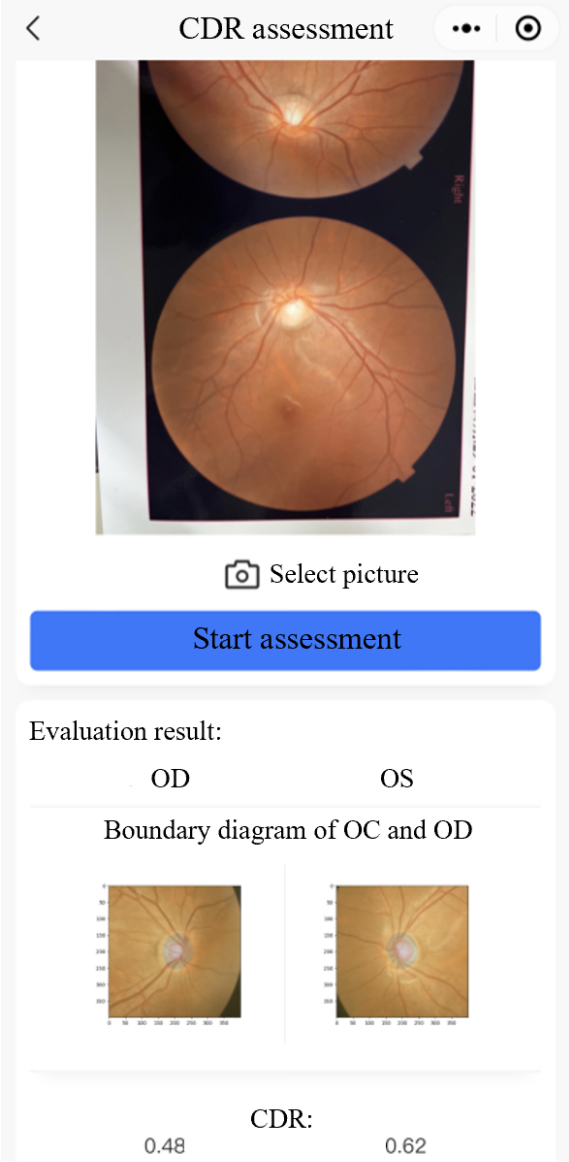

Fig. 6 Interface of our designed WeChat mini-program. Users can choose to upload images from their photo album or capture images using portable devices such as mobile phones or tablets. The lower section displays the segmentation of the OD and OC, as well as the calculation of the CDR after evaluation by the intelligent model. In response to practical requirements from patients, the user interface of our system is designed in Chinese. For the sake of convenience in presentation, we have chosen to display the interface in English.

4.3 Ablation study

We evaluate the usefulness of the newly introduced VC information for CDR segmentation, we utilize the PyTorch framework with identical hyperparameters. We employ SegTran as the baseline model and compared its performance with the addition of key vessel information. Furthermore, to demonstrate the efficacy of glaucoma-induced VC, we incorporate all vessel information learned by the model. The ablation results, depicted in Table 2, indicate that only the glaucoma-induced VC information is beneficial for CDR segmentation.

4.4 Intelligent diagnostic system

We develop a WeChat mini-program to deploy the model, allowing users to upload their original retinal fundus

images or directly capture images of their own cases using the built-in camera. The system diagram is shown in Figure 6. Upon completion of the upload, the intelligent model deployed in the backend automatically performs CDR segmentation and visualizes the results on the user interface, along with the automatic calculation of the CDR. To enhance user experience, we introduce functionalities for retinal photograph localization and automatic classification of left and right eyes. Retinal photograph localization is implemented to accommodate various scenarios. Users may upload retinal fundus images captured under different conditions, which may not be the original images. In such cases, we localize the retinal photographs to the most suitable central regions within the images. Since the positions of the left and right retinal fundus images differ, we facilitate identification by automatically classifying the user-uploaded retinal fundus images and visualizing them as left or right eye images. The user interface of the system is illustrated in Figure 6. The system is used for the screening and diagnosis of glaucoma.

5 Conclusion

In this paper, we incorporate glaucoma-affected VC information into CDR segmentation based on recommendations from clinically experienced doctors. We create the GSD dataset and achieve promising results on both the REFUGE dataset and the GSD dataset. This demonstrates that the curved vessel information surrounding the OD and OC can assist in the segmentation process. By focusing solely on key vessel information, the model reduces the influence of other retinal vessels. Additionally, we design and deploy an intelligent glaucoma diagnosis system. In the future, we will continue to collaborate with hospitals and patients to collect diverse datasets, encompassing various scenarios and more data, to enhance the model's generalization and robustness. We will also optimize and improve the intelligent glaucoma diagnosis system based on user feedback.

6 Acknowledgement

This work is sponsored by the GHfund B (Grant No. 202302028692).

References

1. https://mp.weixin.qq.com/s/vcA_9izdwLwHvC8aL33oBQ
2. World health organization programme for the prevention of blindness and deafness-global initiative for the elimination of avoidable blindness World health organization, Geneva, Switzerland, WHO/PBL/97.61 Rev.1, 1997.
3. Y.-C. Tham et al., "Global prevalence of glaucoma and projections of glaucoma burden through 2040: A systematic review and meta-analysis," Ophthalmology, vol. 121, no. 11, pp. 2081–2090, 2014.
4. D. F. Garway-Heath and R. A. Hitchings, "Quantitative evaluation of the optic nerve head in early glaucoma," Brit. J. Ophthalmol., vol. 82, no. 4, pp. 352–361, 1998.
5. J. B. Jonas, A. Bergua, P. Schmitz-Valckenberg, K. I. Papastathopoulos, and W. M. Budde, "Ranking of optic disc variables for detection of glaucomatous optic nerve damage," Invest. Ophthalmol. Vis. Sci., vol. 41, no. 7, pp. 1764–1773, 2000.
6. A. Almazroa, R. Burman, K. Raahemifar, and V. Lakshminarayanan, "Optic disc and optic cup segmentation methodologies for glaucoma image detection: A survey," J. Ophthalmol., vol. Sep. 2015, Art. no. 180972, 2015.
7. V. Gulshan et al., "Development and validation of a deep learning algorithm for detection of diabetic retinopathy in retinal fundus pho- tographs," J. Amer. Med. Assoc., vol. 316, no. 22, pp. 2402–2410, 2016.
8. Michael D. Hancox O.D., "Optic disc size, an important consideration in the glaucoma evaluation," Clin. Eye Vis. Care, vol. 11, no. 2, pp. 59–62, 1999.
9. M. Wu, T. Leng, L. de Sisternes, D. L. Rubin, and Q. Chen, "Automated segmentation of optic disc in SD-OCT images and cup-to-disc ratios quantification by patch searching-based neural canal opening detection," Opt. Exp., vol. 23, no. 24, pp. 31216–31229, Nov. 2015.
10. K. Lee, M. Niemeijer, M. K. Garvin, Y. H. Kwon, M. Sonka, and M. D. Abràmoff, "Segmentation of the optic disc in 3-D OCT scans of the optic nerve head," IEEE Trans. Med. Imag., vol. 29, no. 1, pp. 159–168, Jan. 2010.
11. H. Fu, D. Xu, S. Lin, D. W. K. Wong, and J. Liu, "Automatic optic disc detection in OCT slices via low-rank reconstruction," IEEE Trans. Biomed. Eng., vol. 62, no. 4, pp. 1151–1158, Apr. 2015.
12. H. Fu et al., "Segmentation and quantification for angle-closure glau- coma assessment in anterior segment OCT," IEEE Trans.Med.Imag., vol. 36, no. 9, pp. 1930–1938, Sep. 2017.
13. A. Krizhevsky, I. Sutskever, and G. E. Hinton, "ImageNet classifica- tion with deep convolutional neural networks," in Proc. NIPS, pp. 1097–1105, 2012.
14. E. Shelhamer, J. Long, and T. Darrell, "Fully convolutional networks for semantic segmentation," IEEE Trans. Pattern Anal. Mach. Intell., vol. 39, no. 4, pp. 640–651, Apr. 2017.
15. Ronneberger O, Fischer P, Brox T. U-net: Convolutional networks for biomedical image segmentation[C]//Medical Image Computing and Computer-Assisted Intervention–MICCAI 2015: 18th International Conference, Munich, Germany, October 5-9, 2015, Proceedings, Part III 18. Springer International Publishing, 2015: 234-241.
16. He K, Gkioxari G, Dollár P, et al. Mask r-cnn[C]//Proceedings of the IEEE international conference on computer vision. 2961-2969, 2017.
17. M. Lalonde, M. Beaulieu, and L. Gagnon, "Fast and robust optic disc detection using pyramidal decomposition and hausdorff-based template matching," IEEE Trans. Med. Imag., vol. 20, no. 11, pp. 1193–1200, Nov. 2001.
18. N. Patton, T. M. Aslam, T. MacGillivray, I. J. Deary, B. Dhillon, R. H.Eikelboom, K. Yogesan, and I. J. Constable,

"Retinal image analysis: Concepts, applications and potential," Progress Retinal Eye Res., vol. 25, no. 1, pp. 99–127, 2006.
19. P. Pallawala, W. Hsu, M. Lee, and K. Eong, "Automated optic disc localization and contour detection using ellipse fitting and wavelet transform," in Proc. ECCV, pp. 139–151, 2004.
20. Wong D W K, Liu J, Lim J H, et al. Automated detection of kinks from blood vessels for optic cup segmentation in retinal images[C]//Medical Imaging 2009: Computer-Aided Diagnosis. SPIE, 7260: 459-466, 2009.
21. Orlando J I, Fu H, Breda J B, et al. Refuge challenge: A unified framework for evaluating automated methods for glaucoma assessment from fundus photographs[J]. Medical image analysis, 59: 101570, 2020.
22. F. Mendels, C. Heneghan, and J. P. Thiran, "Identification of the optic disc boundary in retinal images using active contours," in Proc. IMVIP, 1999.
23. A. Osareh, M. Mirmehdi, B. Thomas, and R. Markham, "Colour morphology and snakes for optic disc localization," in Proc. MIUA, pp. 21–24, 2002.
24. T. Chan and L. Vese, "Active contours without edges," IEEE Trans. Image Process., vol. 10, no. 2, pp. 266–277, Feb., 2001.
25. S. Lee and M. Brady, "Optic disk boundary detection," in Proc. BMVC, pp. 359–3621991.
26. D. Mumford and J. Shah, "Optimal approximation by piecewise smooth functions and associated variational problems," Commun. Pure Appl. Math., vol. 42, pp. 577–685, 1989.
27. J. Lowell, A. Hunter, D. Steel, A. Basu, R. Ryder, E. Fletcher, and L. Kennedy, "Optic nerve head segmentation," IEEE Trans. Med. Imag., vol. 23, no. 2, pp. 256–264, Feb. 2004.
28. J. Novo, M. Penedo, and J. Santos, "Localisation of the optic disc by means of GA-optimised topological active nets," Image Vis. Comput., vol. 27, no. 10, pp. 1572–1584, 2009.
29. H. Li and O. Chutatape, "Boundary detection of optic disk by a mod- ified ASM method," Pattern Recognit., vol. 36, no. 9, pp. 2093–2104, 2003.
30. H. Li and O. Chutatape, "A model based approach for automated fea- ture extraction in fundus images," IEEE Trans. Biomed. Eng., vol. 51, no. 2, pp. 246–254, Feb. 2004.
31. Joshi G D, Sivaswamy J, Krishnadas S R. Optic disk and cup segmentation from monocular color retinal images for glaucoma assessment[J]. IEEE transactions on medical imaging, 30(6): 1192-1205, 2011.
32. Fu H, Cheng J, Xu Y, et al. Joint optic disc and cup segmentation based on multi-label deep network and polar transformation[J]. IEEE transactions on medical imaging, 37(7): 1597-1605, 2018.
33. J. Lowell et al., "Optic nerve head segmentation," IEEE Trans. Med. Imag., vol. 23, no. 2, pp. 256–264, Feb. 2004.
34. A. Sevastopolsky, "Optic disc and cup segmentation methods for glaucoma detection with modification of U-Net convolutional neural network," Pattern Recognit. Image Anal., vol. 27, no. 3, pp. 618–624, 2017.
35. J. Zilly, J. M. Buhmann, and D. Mahapatra, "Glaucoma detection using entropy sampling and ensemble learning for automatic optic cup and disc segmentation," Comput. Med. Imag. Graph., vol. 55, pp. 28–41, Jan. 2017.
36. Zhang Z, Yin F S, Liu J, et al. Origa-light: An online retinal fundus image database for glaucoma analysis and research[C]//2010 Annual international conference of the IEEE engineering in medicine and biology. IEEE, 3065-3068, 2010.
37. Sivaswamy J, Krishnadas S R, Joshi G D, et al. Drishti-gs: Retinal image dataset for optic nerve head (onh) segmentation[C]//2014 IEEE 11th international symposium on biomedical imaging (ISBI). IEEE, 53-56, 2014.
38. Chen J, Lu Y, Yu Q, et al. Transunet: Transformers make strong encoders for medical image segmentation[J]. arXiv preprint arXiv:2102.04306, 2021.
39. Li S, Sui X, Luo X, et al. Medical image segmentation using squeeze-and-expansion transformers[J]. arXiv preprint arXiv:2105.09511, 2021.